N6-Methyladenosine-Related lncRNAs As Potential Biomarkers For Predicting The Prognoses And Immune Responses In Patients With Cervical Cancer

He Zhang
Department of Gynecological Oncology, Beijing Obstetrics and Gynecology Hospital
Weimin Kong (kwm1967@ccmu.edu.cn)
Department of Gynecological Oncology, Beijing Obstetrics and Gynecology Hospital
Chao Han
Department of Gynecological Oncology, Beijing Obstetrics and Gynecology Hospital
Tingting Liu
Department of Gynecological Oncology, Beijing Obstetrics and Gynecology Hospital
Jing Li
Department of Gynecological Oncology, Beijing Obstetrics and Gynecology Hospital
Dan Song
Department of Gynecological Oncology, Beijing Obstetrics and Gynecology Hospital

Research Article

Keywords: m6A, Tumor microenvironment, Stroma, Immunotherapy, Cervical cancer

Posted Date: June 16th, 2021

DOI: https://doi.org/10.21203/rs.3.rs-538180/v1

Version of Record: A version of this preprint was published at BMC Genomic Data on January 18th, 2022.
See the published version at https://doi.org/10.1186/s12863-022-01024-2.

Abstract

Background: Several recent studies have confirmed to us the epigenetic regulation of the immune response. However, the potential role of RNA N6-methyladenosine (m^6A) modifications in cervical cancer and its tumor microenvironment (TME) cell infiltration remains unclear.

Results: We evaluated and analyzed m6A modification patterns in 307 cervical cancer samples from The Cancer Genome Atlas (TCGA) dataset based on 13 m6A regulators. Pearson correlation analysis was used to identify lncRNAs associated with m6A, followed by univariate Cox regression analysis to screen their prognostic role in cervical cancer patients. We also correlated TME cell infiltration characteristics with modification patterns. We screened six m6A-associated lncRNAs as prognostic lncRNAs and established the prognostic profile of m6A-associated lncRNAs by least absolute shrinkage and choice of operator (LASSO) Cox regression. The corresponding risk scores of patients were derived based on their prognostic features, and the correlation between this feature model and disease prognosis was analyzed. The prognostic model constructed based on the TCGA-CESC (The Cancer Genome Cervical squamous cell carcinoma and endocervical adenocarcinoma) dataset showed strong prognostic power in the stratified analysis and was confirmed as an independent prognostic indicator for predicting overall survival of patients with CESC. Principal component analysis showed that low- and high-risk subgroups had significant m^6A status. Enrichment analysis showed that biological processes, pathways, and markers associated with malignancy were more common in the high-risk subgroup. Risk scores were strongly correlated with tumor grade. ECM receptor interaction, pathways in cancer were enriched in cluster 2 while oxidative phosphorylation and other biological processes in cluster 1. The expression of immune checkpoint molecules including PD-1 (programmed death 1) and PD-L1 (programmed death ligand 1) was significantly increased in the high-risk subgroup, suggesting that this prognostic model could be a predictor of immunotherapy.

Conclusions: This study reveals that m^6A modifications play an integral role in the diversity and complexity of TME formation. Assessing the m^6A modification patterns of individual tumors will help improve our understanding of TME infiltration characteristics and thus guide immunotherapy more effectively. We also developed an independent prognostic model based on m^6A-associated lncRNA as a predictor of overall survival, which can also be used as a predictor of immunotherapy.

Background

In all organisms, genetic information flows from DNA to RNA and then to proteins. As the third layer of epigenetics, RNA plays a crucial role, not only in transmitting genetic information from DNA to proteins but also in regulating various biological processes. More than 150 RNA modifications have been identified, including 5-methylcytosine (M5C), N6-methyladenosine (M^6A), and N1-methyladenosine (M1A) among others[1]. Among these modifications, m^6A RNA methylation is considered to be the most dominant and abundant form of internal modification in eukaryotic cells, with an abundance of 0.1–0.4%

of total adenosine residues. m^{6}A RNA methylation is widely present in mRNA, lncRNA, and miRNA[2]. Like DNA and protein modifications, m^{6}A modification is a reversible and dynamic process in mammalian cells, with three major classes of proteins involved in its modification: the first class is the methyltransferases responsible for the modification, the second class is demethylases, and the third class is effector proteins. m^{6}A methylation is formed by RBM15, ZC3H13, METTL3, METTL14, and other methyltransferases, while the removal process is mediated by demethylases such as FTO and ALKBH5[3]. Besides, a group of specific RNA-binding proteins such as YTHDFs, IGF2BPs, and THDC1/2 can recognize m^{6}A motifs and thus affect the function of m^{6}A[4, 5]. An in-depth understanding of these regulatory factors will help to reveal the role and mechanism of m^{6}A modifications in post-transcriptional regulation. It has been reported that m^{6}A regulators play critical roles in a variety of biological functions in vivo. A growing number of studies have shown that aberrant expression and genetic alterations of m^{6}A regulators are associated with a variety of biological processes, including dysregulated cell death and proliferation, developmental defects, malignant tumor progression, impaired self-renewal capacity, and abnormal immune regulation[6–8].

Using the immune system to fight cancer has become an effective treatment option, and immunotherapy represented by immune checkpoint blockade (ICB, PD-1/L1, and CTLA-4) has shown impressive clinical efficacy in several cancer types[9, 10]. Unfortunately, the clinical benefit for most patients remains relatively small and far from what is needed to satisfy clinicians. Traditionally we have considered tumor progression to be a multistep process involving only genetic and epigenetic variation in tumor cells[11]. However, numerous studies have shown that the microenvironment, on which tumor cells grow and survive, also plays a crucial role in tumor progression. The tumor microenvironment (TME) contains not only cancer cells, but also stromal cells (e.g., resident fibroblasts, cancer associated fibroblast (CAF)) and macrophages, as well as distantly recruited cells such as infiltrating immune cells (myeloid and lymphocytes), bone marrow-derived cells (BMDCs), and secreted factors such as cytokines, chemokines, growth factors, and neointima[12]. With the increasing understanding of the diversity and complexity of the tumor microenvironment, there is growing evidence that the tumor microenvironment plays an important role in tumor progression, immune escape, and its impact on immunotherapeutic response[13]. Predicting ICB response based on the characteristics of TME cell infiltration is a critical step to improve the success of existing ICBS and to develop new immunotherapeutic strategies[14]. Thus, by synthesizing the heterogeneity and complexity of the TME landscape, it is possible to identify distinct tumor immunophenotypes and the ability to guide and predict immunotherapeutic responses will be improved. Also, we hope to reveal new relevant biomarkers and hopefully demonstrate the effectiveness of these markers in identifying patient responses to immunotherapy and will help us to find new relevant therapeutic targets.

In recent years, several studies have proposed a correlation between TME immune cell infiltration and m^{6}A modifications[15]. Some evidence has demonstrated that m^{6}A regulates transcriptional and protein expression through splicing, translation, degradation, and export, thereby mediating the biological

processes of cancer cells and/or stromal cells and characterizing the TME[16]. TME also plays a critical role in the complex regulatory network of m^{6}A modifications and subsequently affects tumorigenesis, progression, and therapeutic response[17]. Wang et al. showed that RNA methyltransferase METTL3-mediated m^{6}A methylation promotes dendritic cell (DC) activation and function. m^{6}A translation of the METTL3-mediated CD40, CD80, and TLR4 signaling junctions TIRAP transcripts is enhanced in DCs to stimulate T cell activation and enhances TLR4/NF-κB signaling-induced cytokine production[5]. Research by Jiang et al. showed that highly expressed TLR4 activated NF-κB pathway, up-regulated ALKBH5 expression, and increased m^{6}A level and NANOG expression, all contributing to ovarian carcinogenesis[18]. Chen et al. showed that m^{6}A methylation of RNA and HIF-1α/2α-dependent AlkB homologue 5 (ALKBH5) participate in the regulation of HIFs and SOX2 in endometrial carcinoma. Hypoxia induces an endometrial cancer stem-like cell phenotype via HIF-dependent demethylation of SOX2 mRNA[19]. However, studies on the relationship between m^{6}A and TMB interactions in cervical cancer have been rarely reported.

In general, basic research may be limited to only one or two M^{6}A regulators and cell types. However, it is well known that antitumor effects are characterized by the interaction and high synergy of numerous tumor suppressors. Therefore, a comprehensive understanding of multiple m^{6}A regulators mediated TME cell infiltration patterns will help deepen our understanding of TME immune regulation[20]. In this study, we integrated genomic information from 307 cervical cancer specimens, performed a comprehensive evaluation of M^{6}A modification patterns, and correlated M^{6}A modification patterns with TME cell infiltration characteristics. We established an m^{6}A-related lncRNA-based scoring system to quantify the m^{6}A modification patterns of individual patients.

Methods

Cervical cancer dataset source and preprocessing

The workflow of our study was shown in **Figure 1**. Public gene-expression data and full clinical annotation were searched in the TCGA database. Patients without survival information were removed from further evaluation. TCGA-CESC was gathered in this study for further analysis, which included a total of 307 patients with cervical cancer. RNA sequencing data (FPKM value) of gene expression were downloaded from the Genomic Data Commons (GDC, https://portal.gdc.cancer.gov/)[21]. Then FPKM values were transformed into transcripts per kilobase million (TPM) values. Co-expression analysis of m^{6}A-associated genes and lncRNA-associated genes using the "limma" package. Construction of gene co-expression network relationship graphs using the "igraph" package.

Unsupervised clustering for 13 m^{6}A regulators

A total of 13 regulators were extracted from TCGA datasets for identifying different m^{6}A modification patterns mediated by m^{6}A regulators. These 13 m^{6}A regulators included 6 writers (METTL3, METTL14,

RBM15, WTAP, KIAA1429, ZC3H13), 2 erasers (ALKBH5, FTO), and 5 readers (YTHDC1, YTHDC2, YTHDF1, YTHDF2, HNRNPC). Unsupervised clustering analysis was applied to identify distinct m^6A modification patterns based on the expression of 6 m^6A regulators and classify patients for further analysis. The number of clusters and their stability were determined by the consensus clustering algorithm. We used the R package “ConsensuClusterPlus” to perform the above steps and 1000 times repetitions were conducted for guaranteeing the stability of classification[22].

Estimation of TME cell infiltration and functional annotation

We used the GSEA (gene-set enrichment analysis) algorithm to quantify the relative abundance of each cell infiltration in the CESC TME, including activated CD8 T cell, activated dendritic cell, macrophage, natural killer T cell, regulatory T cell, and so on. GSEA was performed using the GSEA software, and gene sets of “c2.cp.kegg.v7.2.symbols” were downloaded from the MSigDB database(http://software.broadinstitute.org/gsea/msigdb) for running GSEA analysis. The enrichment scores calculated by GSEA analysis were utilized to represent the relative abundance of each TME infiltrating cell in each sample. We regarded the pathways with |NES|>1, NOM p-val < 0.05 as significantly enriched pathways.

Construction of the Prognostic Signature

The m^6A methylation regulators were included in the Least Absolute Shrinkage and Selection Operator (LASSO) Cox regression model. Prognostic features and correlation models were constructed and their correlation coefficients were calculated, and the expression of each gene was multiplied by its coefficient to calculate the sum of risk scores for each patient. The sensitivity and specificity of the prognostic signature were accessed by receiver operating characteristic (ROC) curves and area under the ROC curves (AUC).

Statistical analysis

The survival curves for the prognostic analysis were generated via the Kaplan-Meier method and log-rank tests were utilized to identify the significance of differences. We adopted a univariate Cox regression model to calculate the hazard ratios (HR) for m^6A regulators and m^6A phenotype-related genes. The independent prognostic factors were ascertained through a multivariable Cox regression model. Patients with detailed clinical data were eligible for final multivariate prognostic analysis. The forest plot R package was employed to visualize the results of multivariate prognostic analysis for m^6Ascore in TCGA-CESC cohort. The specificity and sensitivity of m^6Ascore were assessed through the ROC curve, and the AUC was quantified using “timeROC” R package. All statistical P value were two sides, with $p < 0.05$ as statistically significant. All data processing was done in R 4.0.4 software.

Conclusion

Expression, Correlation, and Interaction of M^6A methylation regulators in cervical cancer

The mRNA expression levels of m^6A RNA methylation regulators were analyzed using transcriptome data in FPKM format. The expression levels of different m^6A genes in normal and tumor tissues were observed and analyzed differently by heat map from R package "pheatmap" **(Fig. 2C)**, and we also showed the differential expression of 13 regulators between CESC and normal tissues by correlation map from R package "corrplot" **(Fig. 2B)** and violin map from "vioplot" **(Fig. 2A)**. The results showed that the regulators were positively correlated with each other, including a significant positive correlation between YTHDC1 and METTL14 with a correlation coefficient of 0.63. The mRNA expression levels of three regulators (RBM15, METTL3, and YTHDF2) were significantly increased, and FTO was decreased in CESC compared with normal tissues. No significant difference was found for the other nine regulators.

Co-expression of m^6A and its relationship with lncRNAs, and search for prognosis-related lncRNAs

Although the functions of most lncRNAs are currently not fully determined, synergistic regulatory relationships or functional correlations between lncRNAs and mRNAs have been suggested to exist. Therefore, by constructing a co-expression network of lncRNAs and mRNAs, we can predict the possible role of lncRNAs in cervical cancer. The m^6A-related lncRNAs were identified by co-expression analysis with the R package "limma". m^6A and lncRNA co-expression relationships were plotted with the R package "igraph". Six prognosis-associated lncRNAs, AC008124.1 ($p = 0.04$, HR = 0.668), AC015922.2 ($p = 0.005$, HR = 1.093), AC073529.1, C9orf147, AC000068.1, and RPP38-DT ($p < 0.1$) were analyzed and identified in combination with clinical survival data. The high-risk lncRNAs associated with prognosis are indicated in red and the low-risk ones are indicated in green. lncRNA heat maps and box plots were obtained by the R packages "pheatmap", "reshape2" and "ggpubr".

Consensus Clustering Identified Two Clusters of CESC

The CESC cohort can be divided into clusters based on the consistency of lncRNA expression of the 13 m^6A RNA methylation regulators. When the cluster index "k" was increased from 2 to 9, k = 2 proved to be the best point to obtain the maximum difference between clusters and the least interference between clusters at this time. The CESC cohort was then divided into Cluster 1 and Cluster 2, where cluster 2 represents a higher lncRNA score. However, no significant survival difference was found between the two groups by Kaplan-Meier survival analysis ($p = 0.066$).

Clinical features between the clusters

Then the correlation between the two clusters and clinical characteristics were analyzed as shown in the figure, we explored the relationship between the six lncRNAs mentioned above and TNM stage, FIGO (Federation International of Gynecology and Obstetrics), stage, age, and grading, but the results showed that the correlation between them was not significant ($p>0.05$).

Analysis of immune cell infiltration in CESC

The R package "CIBERSORT" was used to obtain the results of the immune cell content in the CESC samples, and to score the stromal cells and immune cells in the samples separately. The total score of both is the combined score, i.e. CIBERSORT score. Violin plots (**Fig. 5A**) and box plots (**Fig. 5B**) of immune cell differences between clusters were plotted using the R package "vioplot" and "ggpubr". Differential analysis of immune cells between clusters showed that T cells CD4 memory activated($p = 0.016$), T cells gamma delta($p = 0.008$) and Dendritic cells resting($p = 0.022$) were highly expressed in Cluster 1 compared to Cluster 2, And T cells CD4 memory resting($p = 0.049$) was highly expressed in Cluster2 compared to Cluster1. But the scoring of the tumor microenvironment between the two clusters was not statistically significant.

Results of CESC tumor microenvironment enrichment analysis

Next, considering the strong association between m^6A-associated lncRNA scores and prognostic and clinical features, we identified genes and signaling pathways associated with m^6A-related lncRNAs that influence clinical outcomes. We have used the KEGG (Kyoto Encyclopedia of Genes and Genomes) database to apply GSEA to examine the rich set of genes from both clusters (**Fig. 6**). ECM receptor interaction (NES (normalized enrichment score) = 1.67, Nominal p = 0.03), pathways in cancer (NES = 1.61, Nominal p = 0.006), and other biological processes were enriched in cluster 2 while oxidative phosphorylation and other biological processes in cluster 1. Some of these gene sets were previously identified as being related to m^6A modification. These results may give us some insight into the biological effects of m^6A-related lncRNAs.

Development of a Prognostic Signature

A prognostic signature, including AC008124.1, RPP38-DT, AC015922.2, and AC073529.1 was developed using the LASSO Cox regression model according to the minimum criterion **(Fig. 7A, B)**. The coefficients of AC008124.1, RPP38-DT, AC015922.2 and AC073529.1 were − 0.4945, -0.7024, 0.0962 and − 1.6514 respectively. The risk score for each CESC patient was therefore calculated with the following formula:

$$riskScore= \sum (Coef_i * lncRNA_i)$$

where i is the expression of m^6A-related lncRNA.

To validate the prognostic value of this model, we divided the training (n=152) and testing (n=152) cohorts into high- and low-risk groups based on significant differences in OS determined by Kaplan–Meier curves ($p_{training}<0.01$, $p_{testing}<0.05$) **(Figure 7E, F)**. Based on area under the curve (AUC) values, the model adequately predicted OS rates for CESC patients in both cohorts ($AUC_{training}=0.708$, $AUC_{testing}=0.668$) **(Figure 7C, D)**. Risk profiles for the train and test groups showed that AC015922.2 was highly expressed in the high-risk group, while RPP38-DT, AC008124.1, and AC073529.1 were highly expressed in the low-risk group **(Figure 8)**.

m^6A risk scores as independent prognostic indicators

To further evaluate the prognostic value of the m^{6}A-related lncRNA risk signature, factors including risk score, age, FIGO stage, and histological grade were successively included in univariate and multivariate Cox regression models. Because the training and testing cohorts were derived from the same datasets and the sample size was limited, we subsequently merged all samples to increase the sample size. Univariate and multifactorial Cox regression analyses showed that the risk score and stage were significantly related to OS in both Cox analyses ($p < 0.001$) **(Fig. 9A, B)**, indicating that the signature may be an independent prognostic tool.

Association between m^{6}A-related lncRNA risk scores and clinicopathological characteristics

Next, we evaluated the association between risk scores and clinicopathological features by producing a heatmap of clinical characteristics including TNM stage, histological grade, and FIGO stage, associated with expression levels of the four selected regulators, where the immune score, cluster, differed between patients in high and low-risk groups **(Fig. 9C)**. no significant differences were detected among other clinical characteristics. Validation of the grouping by grading, staging, and age showed that the model we developed applied to different clinical groupings including age < 50 ($p = 0.04$), age > = 50 ($p = 0.004$), Stage IA-IIA ($p < 0.001$), G1-G2 ($p = 0.046$), G2-G3 ($p = 0.006$). There were statistically significant differences in patient risk between age groups (age > = 50/age < 50, $p = 0.047$), immune scoring (high/low, $p = 0.002$), and clusters (cluster1/2, $p = 1.3e^{*-10}$), and no statistically significant differences between patients with different staging and grading **(Fig. 9D)**.

Identification of m^{6}A-related lncRNA risk scores associated with immune checkpoint molecules and immune cells

Next, we analyzed the effects of m^{6}A-related lncRNA modification on immune responses in CESC patients. The m^{6}A-related high-risk subgroup was associated with significantly higher expression of several immune checkpoints, including PD-1 (programmed death 1) and PD-L1 (programmed death-ligand 1) **(Fig. 10A)**. However, the correlation with CTLA-4 (cytotoxic T-lymphocyte–associated antigen 4) was not significant. For immune cells in the tumor microenvironment, Mast cells activated ($p = 0.002$), Neutrophils ($p = 0.045$) and NK cells resting ($p = 0.026$) were positively associated with patients' risk, and B cells naive ($p < 0.01$), Dendritic cells resting ($p = 0.032$) and Mast cells resting ($p = 0.003$) were negatively correlated with patient risk **(Fig. 10B)**. These findings suggest that our score may predict the efficacy of immunotherapy in CESC patients. This finding needs to be further validated and confirmed in our clinical practice.

Discussion

As a reversible RNA modification process, m^{6}A methylation has recently attracted much attention. However, how it plays a role in the development of cervical cancer in a lncRNA-dependent manner is still unknown[23, 24]. A growing body of research evidence suggests that m^{6}A modification plays an important role in immune response, inflammation, and antitumor effects by interacting with different m^{6}A

regulators[25]. Although a large number of studies have revealed the epigenetic regulatory role of m^{6}A regulators in the immune environment, the overall characterization of m^{6}A regulator mediated TME has not been fully understood[26, 27]. Therefore, identifying different m^{6}A modification patterns in the tumor immune microenvironment will help provide insight into the interactions of m^{6}A methylation in the antitumor immune response and help clinicians develop more precise tumor immunotherapy strategies[20, 28].

A total of 307 cervical cancers from the TCGA database were included in our study to explore the prognostic significance of m^{6}A-associated tumor microenvironment and lncRNAs. Four m^{6}A-associated lncRNAs, AC008124.1, RPP38-DT, AC015922.2, and AC073529.1 were shown to have prognostic value in the TCGA dataset. Several of the four lncRNAs have been reported to be associated with cancer progression, among them, Zhou et al. reported that the lncRNA AC008124.1 competes with mRNA to perform its function in different breast cancer subtypes[29]. Evans et al. suggest that lncRNA RPP38-DT may play a function in non-small cell lung cancer[30]. Expression of lncRNA AC015922.2 has been suggested to be possibly associated with metastasis and higher pathological grade in renal clear cell carcinoma[31]. However, there are few reports on cervical cancer and even fewer reports on how lncRNAs interact with m^{6}A-related genes. Our study shows that these lncRNAs compete with different mRNAs for their functions in regulating the activities of different cervical cancer cells.

We scored the CESC cohort patients according to their high or low expression of m^{6}A-related lncRNAs and analyzed the established independent prognostic model showing that patients with higher scores were usually accompanied by lower OS and worse clinical outcomes, a finding that held in patients with cervical cancer of different grades, age > 50 years, age < 50 years and early stages. In the analysis of the tumor immune microenvironment, some studies point out that TME shapes the fate of tumors by modulating the dynamic DNA (and RNA) methylation patterns of these immune cells to alter their differentiation into pro-cancer (e.g., regulatory T cells) or anti-cancer (e.g., CD8 + T cells) cell types[32]. We found that high-risk subgroups were significantly associated with elevated levels of tumor-infiltrating lymphocytes and PD-L1 and PD-1, supporting the potential predictive value for immunotherapy.

The results of this study were derived and validated using the TCGA dataset for cervical cancer, but several limitations of our study remain. More independent cervical cancer cohorts should be used to validate the prognosis of m^{6}A-associated lncRNAs. In addition, the role of lncRNAs and their interactions with m^{6}A-related genes should be experimented with and confirmed using in vitro and in vivo approaches.

In summary, our study comprehensively evaluated the M^{6}A modification patterns of 13 M^{6}A regulators in 307 cervical cancer samples, established an independent prognostic model based on m^{6}A-associated lncRNAs, and systematically correlated these modification patterns with TME cell infiltration characteristics. The above evidence suggests that m^{6}A modifications are targeted to lncRNAs and that RNA methylation lays an important foundation for immune regulation of tumors. Assessing the m^{6}A modification patterns of individual tumors will help improve our understanding of the infiltrative

characteristics of TME. We should pay more attention to the interaction and function of lncRNAs with m^6A modifications to identify potential cervical cancer prognostic markers or therapeutic targets. Therefore, we hope that our findings will help identify prognostic lncRNAs that may be targeted by m^6A modulators, thereby providing insight into their potential role in cervical cancer development, which can be applied to clinical practice to guide treatment options.

Abbreviations

m^6A: RNA N6-methyladenosine; TME:tumor microenvironment; TCGA:The Cancer Genome Atlas; LASSO:absolute shrinkage and choice of operator; TCGA:The Cancer Genome Cervical squamous cell carcinoma and endocervical adenocarcinoma; PD-1:programmed death 1; PD-L1:programmed death ligand 1; M5C:5-methylcytosine; M1A:N1-methyladenosine; ICB:immune checkpoint blockade; CAF:cancer associated fibroblast; BMDCs:bone marrow-derived cells; DC:dendritic cell; GEO:Gene-Expression Omnibus; GSEA:gene-set enrichment analysis; ROC:receiver operating characteristic; AUC:area under the ROC curves; HR:hazards ratio; OR:odds ratio; Figo:Federation International of Gynecology and Obstetrics; KEGG:Kyoto Encyclopedia of Genes and Genomes.

Declarations

Ethics approval and consent to participate

Not applicable. Though the results contain analyses using publicly available data obtained TCGA.

Consent for publication

Not applicable.

Availability of data and materials

The datasets generated during and analyzed during the current study are available in The Cancer Genome Atlas repository (https://portal.gdc.cancer. gov/). The source codes supporting the conclusions of this article are available in the GitHub at https://github.com/zhanghe54321/m6acervival.git.

Competing Interests

The authors declare that they have no conflict of interest.

Funding

This study does not include any funding support.

Author contributions

HZ and WMK contributed significantly to analysis and manuscript preparation, performed the data analyses, and wrote the manuscript. WMK contributed to the conception of the study. CH, TTL, JL and DS helped perform the analysis with constructive discussions. All authors read and approved the final manuscript.

Acknowledgments

The authors would like to thank colleagues at Beijing Obstetrics and Gynecology Hospital at Capital Medical University for providing feedback. Thanks to RHZ, FZZ for their contribution to this study of statistical research.

Author lists

He Zhang[1, 2], Weimin Kong[1, 2*], Chao Han[1, 2], Tingting Liu[1, 2] Jing Li[1, 2], Dan Song[1, 2]

[*]Correspondence: Weimin Kong. Email: kwm1967@ccmu.edu.cn

[1] Department of Gynecological Oncology, Beijing Obstetrics and Gynecology Hospital, Capital Medical University, Beijing 100006, China.

[2] Department of Gynecological Oncology, Beijing Maternal and Child Health Care Hospital, Beijing 100006, China.

References

[1] Roundtree I A, Evans M E, Pan T, et al. Dynamic RNA Modifications in Gene Expression Regulation[J]. Cell, 2017, 169(7): 1187-1200. doi:10.1016/j.cell.2017.05.045.

[2] Ma S, Chen C, Ji X, et al. The interplay between m6A RNA methylation and noncoding RNA in cancer[J]. J Hematol Oncol, 2019, 12(1): 121. doi:10.1186/s13045-019-0805-7.

[3] Wang Q, Chen C, Ding Q, et al. METTL3-mediated m(6)A modification of HDGF mRNA promotes gastric cancer progression and has prognostic significance[J]. Gut, 2020, 69(7): 1193-1205. doi:10.1136/gutjnl-2019-319639.

[4] Fu Y, Dominissini D, Rechavi G, et al. Gene expression regulation mediated through reversible m^6A RNA methylation[J]. Nat Rev Genet, 2014, 15(5): 293-306. doi:10.1038/nrg3724.

[5] Wang H, Hu X, Huang M, et al. Mettl3-mediated mRNA m(6)A methylation promotes dendritic cell activation[J]. Nat Commun, 2019, 10(1): 1898. doi:10.1038/s41467-019-09903-6.

[6] Zhao B S, Roundtree I A, He C. Post-transcriptional gene regulation by mRNA modifications[J]. Nat Rev Mol Cell Biol, 2017, 18(1): 31-42. doi:10.1038/nrm.2016.132.

[7] Lin X, Chai G, Wu Y, et al. RNA m(6)A methylation regulates the epithelial mesenchymal transition of cancer cells and translation of Snail[J]. Nat Commun, 2019, 10(1): 2065. doi:10.1038/s41467-019-09865-9.

[8] Rodriguez-Ruiz M E, Vitale I, Harrington K J, et al. Immunological impact of cell death signaling driven by radiation on the tumor microenvironment[J]. Nat Immunol, 2020, 21(2): 120-134. doi:10.1038/s41590-019-0561-4.

[9] Minn A J, Wherry E J. Combination Cancer Therapies with Immune Checkpoint Blockade: Convergence on Interferon Signaling[J]. Cell, 2016, 165(2): 272-5. doi:10.1016/j.cell.2016.03.031.

[10] Topalian S L, Taube J M, Pardoll D M. Neoadjuvant checkpoint blockade for cancer immunotherapy[J]. Science, 2020, 367(6477). doi:10.1126/science.aax0182.

[11] Quail D F, Joyce J A. Microenvironmental regulation of tumor progression and metastasis[J]. Nat Med, 2013, 19(11): 1423-37. doi:10.1038/nm.3394.

[12] Vitale I, Manic G, Coussens L M, et al. Macrophages and Metabolism in the Tumor Microenvironment[J]. Cell Metab, 2019, 30(1): 36-50. doi:10.1016/j.cmet.2019.06.001.

[13] Goliwas K F, Deshane J S, Elmets C A, et al. Moving Immune Therapy Forward Targeting TME[J]. Physiol Rev, 2021, 101(2): 417-425. doi:10.1152/physrev.00008.2020.

[14] Deberardinis R J. Tumor Microenvironment, Metabolism, and Immunotherapy[J]. N Engl J Med, 2020, 382(9): 869-871. doi:10.1056/NEJMcibr1914890.

[15] Li M, Zha X, Wang S. The role of N6-methyladenosine mRNA in the tumor microenvironment[J]. Biochim Biophys Acta Rev Cancer, 2021, 1875(2): 188522. doi:10.1016/j.bbcan.2021.188522.

[16] Zhu J, Xiao J, Wang M, et al. Pan-Cancer Molecular Characterization of m(6)A Regulators and Immunogenomic Perspective on the Tumor Microenvironment[J]. Front Oncol, 2020, 10: 618374. doi:10.3389/fonc.2020.618374.

[17] Gu Y, Wu X, Zhang J, et al. The evolving landscape of N(6)-methyladenosine modification in the tumor microenvironment[J]. Mol Ther, 2021. doi:10.1016/j.ymthe.2021.04.009.

[18] Jiang Y, Wan Y, Gong M, et al. RNA demethylase ALKBH5 promotes ovarian carcinogenesis in a simulated tumour microenvironment through stimulating NF-κB pathway[J]. J Cell Mol Med, 2020, 24(11): 6137-6148. doi:10.1111/jcmm.15228.

[19] Chen G, Liu B, Yin S, et al. Hypoxia induces an endometrial cancer stem-like cell phenotype via HIF-dependent demethylation of SOX2 mRNA[J]. Oncogenesis, 2020, 9(9): 81. doi:10.1038/s41389-020-00265-z.

[20] Kaymak I, Williams K S, Cantor J R, et al. Immunometabolic Interplay in the Tumor Microenvironment[J]. Cancer Cell, 2021, 39(1): 28-37. doi:10.1016/j.ccell.2020.09.004.

[21] Colaprico A, Silva T C, Olsen C, et al. TCGAbiolinks: an R/Bioconductor package for integrative analysis of TCGA data[J]. Nucleic Acids Res, 2016, 44(8): e71. doi:10.1093/nar/gkv1507.

[22] Wilkerson M D, Hayes D N. ConsensusClusterPlus: a class discovery tool with confidence assessments and item tracking[J]. Bioinformatics, 2010, 26(12): 1572-3. doi:10.1093/bioinformatics/btq170.

[23] Liu T, Wei Q, Jin J, et al. The m6A reader YTHDF1 promotes ovarian cancer progression via augmenting EIF3C translation[J]. Nucleic Acids Res, 2020, 48(7): 3816-3831. doi:10.1093/nar/gkaa048.

[24] Barbieri I, Kouzarides T. Role of RNA modifications in cancer[J]. Nat Rev Cancer, 2020, 20(6): 303-322. doi:10.1038/s41568-020-0253-2.

[25] Han D, Liu J, Chen C, et al. Anti-tumour immunity controlled through mRNA m(6)A methylation and YTHDF1 in dendritic cells[J]. Nature, 2019, 566(7743): 270-274. doi:10.1038/s41586-019-0916-x.

[26] He L, Li H, Wu A, et al. Functions of N6-methyladenosine and its role in cancer[J]. Mol Cancer, 2019, 18(1): 176. doi:10.1186/s12943-019-1109-9.

[27] Chen X Y, Zhang J, Zhu J S. The role of m(6)A RNA methylation in human cancer[J]. Mol Cancer, 2019, 18(1): 103. doi:10.1186/s12943-019-1033-z.

[28] Huang H, Weng H, Chen J. m(6)A Modification in Coding and Non-coding RNAs: Roles and Therapeutic Implications in Cancer[J]. Cancer Cell, 2020, 37(3): 270-288. doi:10.1016/j.ccell.2020.02.004.

[29] Zhou S, Wang L, Yang Q, et al. Systematical analysis of lncRNA-mRNA competing endogenous RNA network in breast cancer subtypes[J]. Breast Cancer Res Treat, 2018, 169(2): 267-275. doi:10.1007/s10549-018-4678-1.

[30] Evans R E. Survival and Biomarker Trends for Non-small Cell Lung Cancer with the Implementation of Cuban Developed Therapies[D]. State University of New York at Buffalo, 2020.

[31] Yang W, Zhou J, Zhang K, et al. Identification and validation of the clinical roles of the VHL-related LncRNAs in clear cell renal cell carcinoma[J], 2021, 12(9): 2702-2714.

[32] Mehdi A, Rabbani S A. Role of Methylation in Pro- and Anti-Cancer Immunity[J]. Cancers (Basel), 2021, 13(3). doi:10.3390/cancers13030545.

Figures

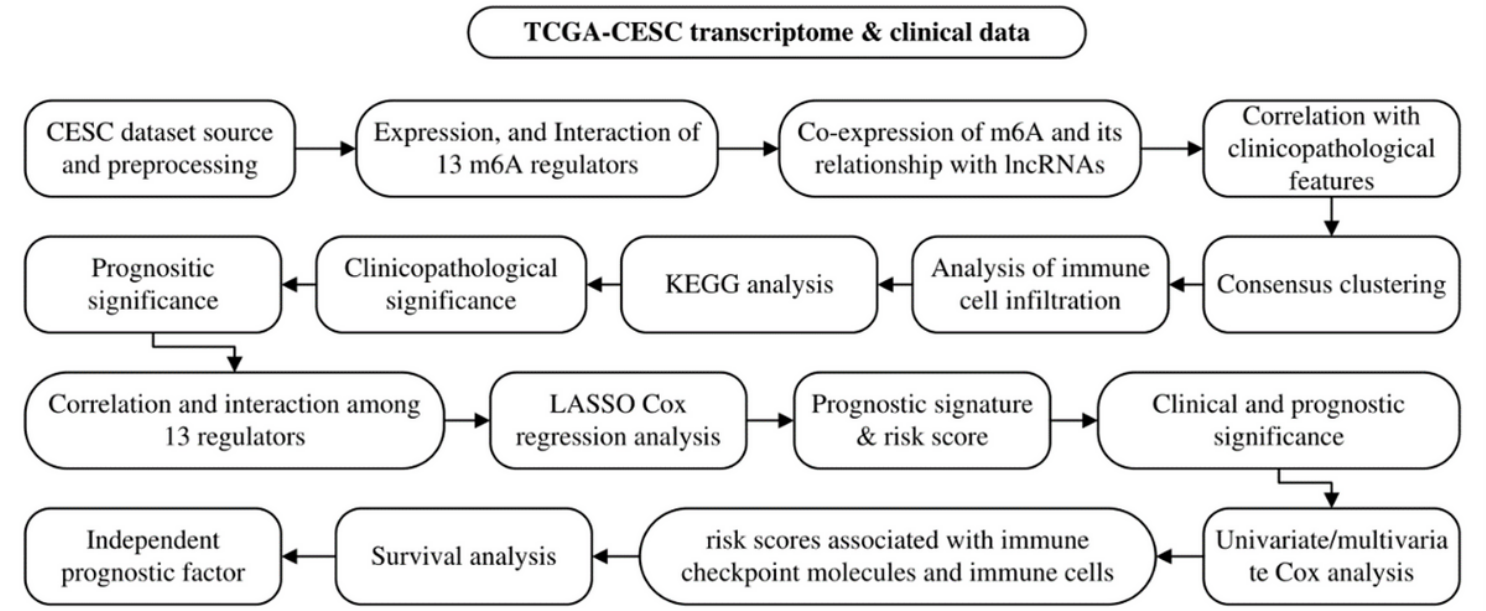

Figure 1

Flow chart of development and validation of an N6-methylandenosine-related lncRNAs based prognostic signature for CESC.

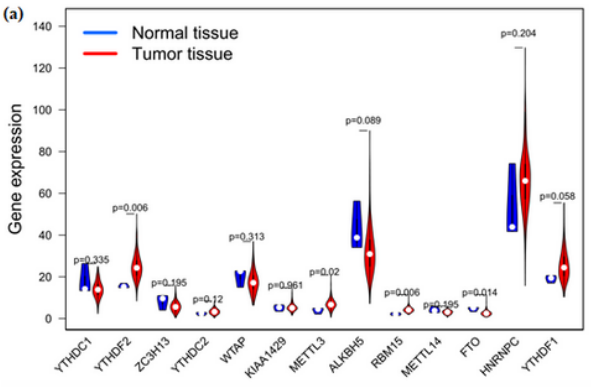

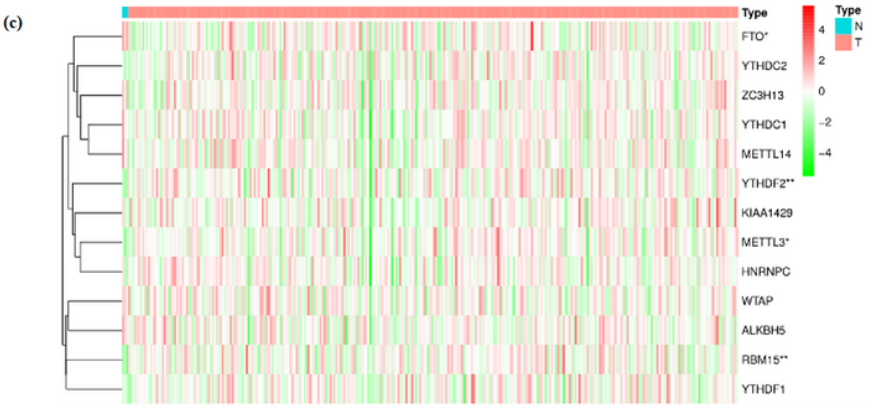

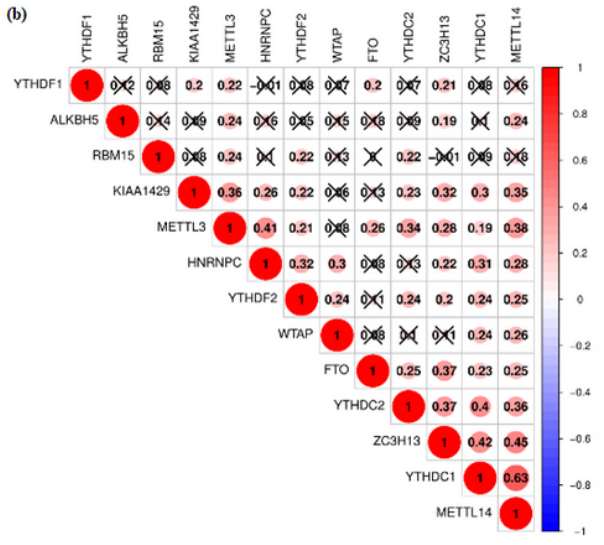

Figure 2

The expression of 13 m6A RNA methylation regulators in TCGA-CESC cohort. (A) The violin plot showed the significantly differentially expressed m6A RNA methylation regulators between CESC tissues and the normal tissues. (B) The correlations among m6A RNA methylation regulators were analyzed by Pearson correlation. (C) The heatmap among m6A RNA methylation regulators between CESC tissues and the normal tissues.

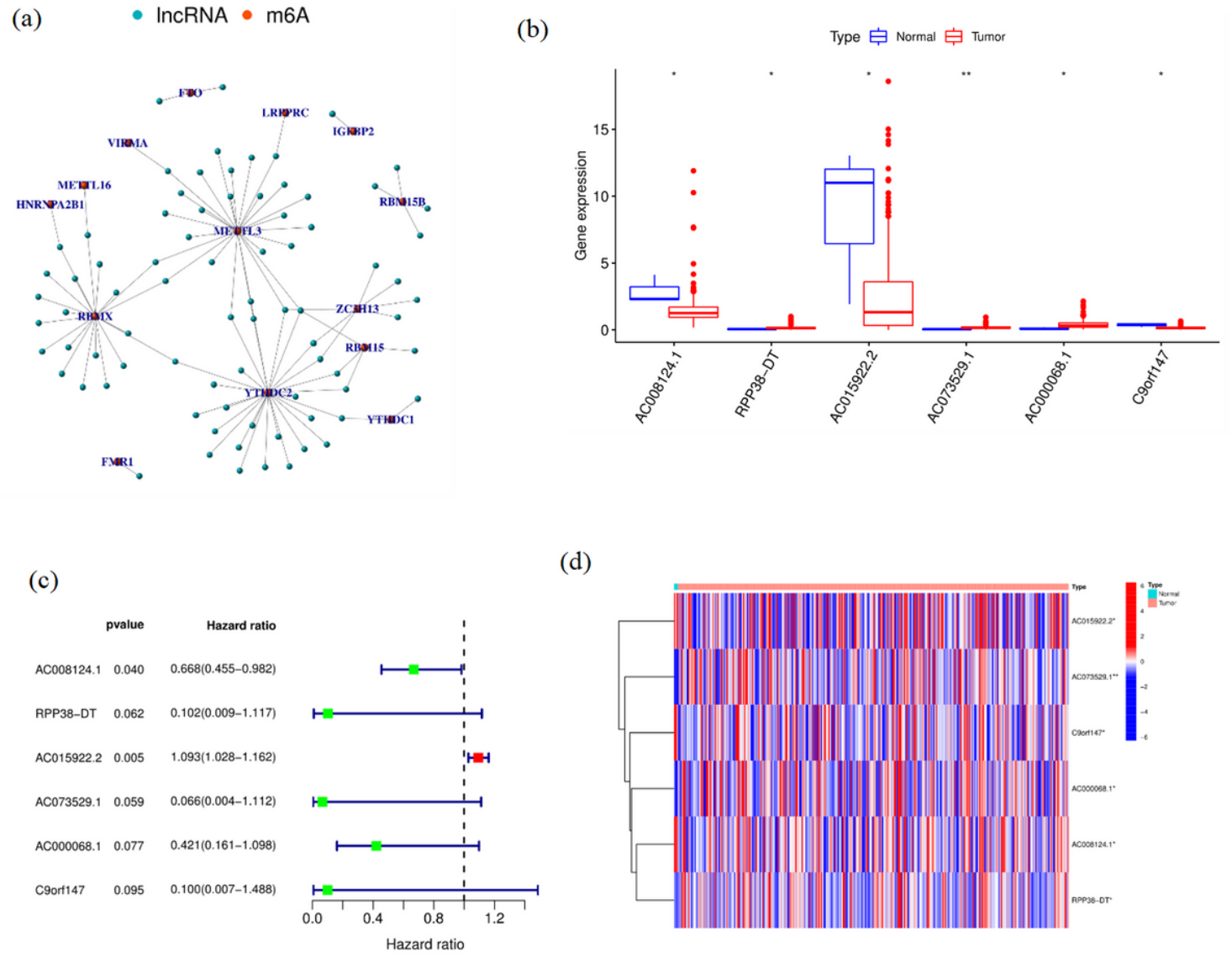

Figure 3

(A) Co-expression of m6A and its relationship with lncRNAs. (B) Expression of target lncRNAs in tumor samples and normal samples. (C) Forest plot of lncRNA expression by one-way cox analysis, where red represents high-risk lncRNAs and green represents low-risk lncRNAs ($p<0.1$). (D) Heat map of lncRNA expression in normal and tumor samples, red represents up-regulated expression, blue represents down-regulated expression.

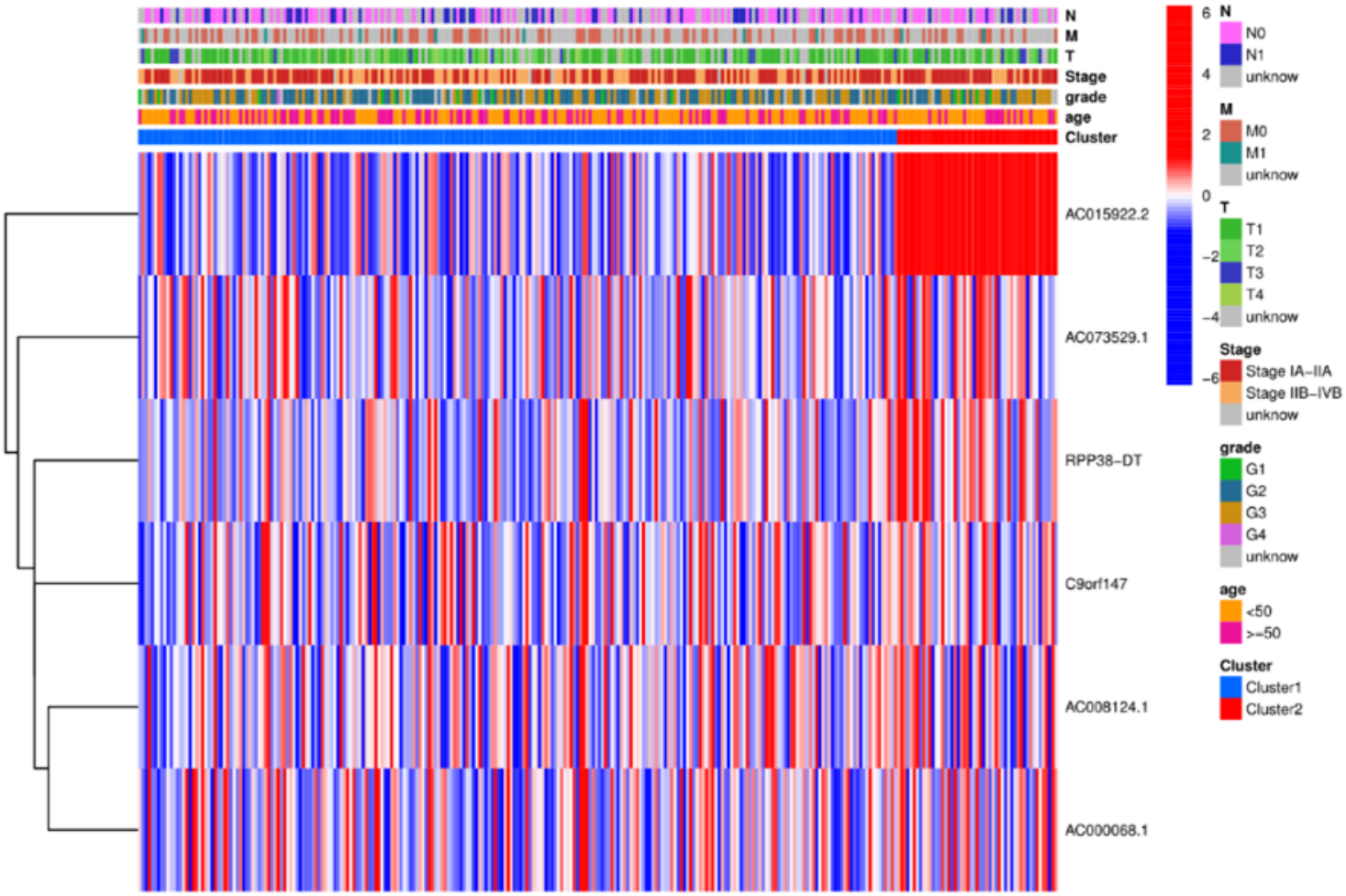

Figure 4

Clinical features (including TNM staging, early (IA-IIA) and late (IIB-IVB) FIGO staging, histological grading, age >50 years/< 50 years, and clusters 1/2.

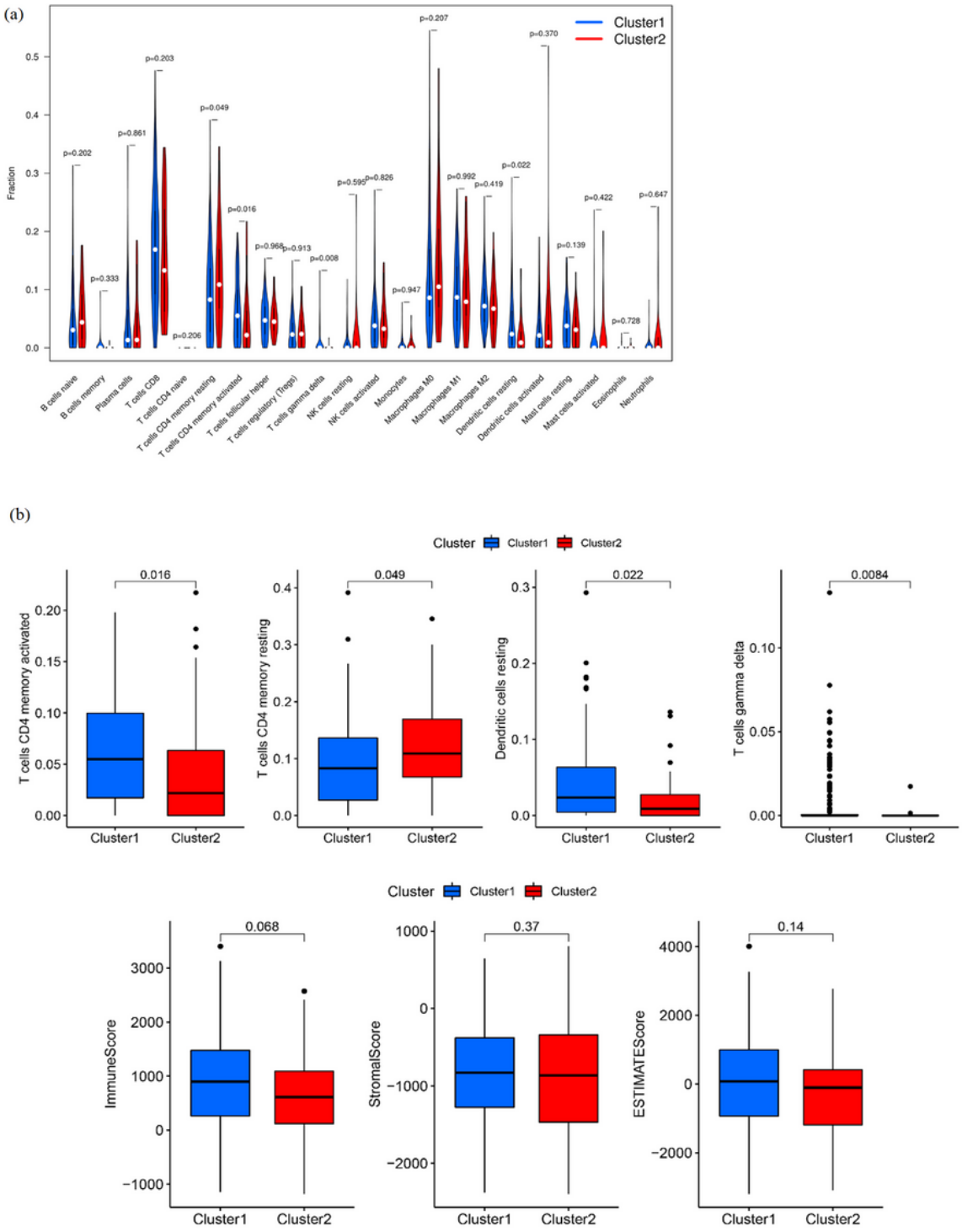

Figure 5

Analysis of immune cell infiltration in CESC. (A) Violin plots of immune cell differences between clusters 1/2. (B) Box plots of immune cell differences between clusters 1/2. Where blue represents cluster 1 and red represents cluster 2.

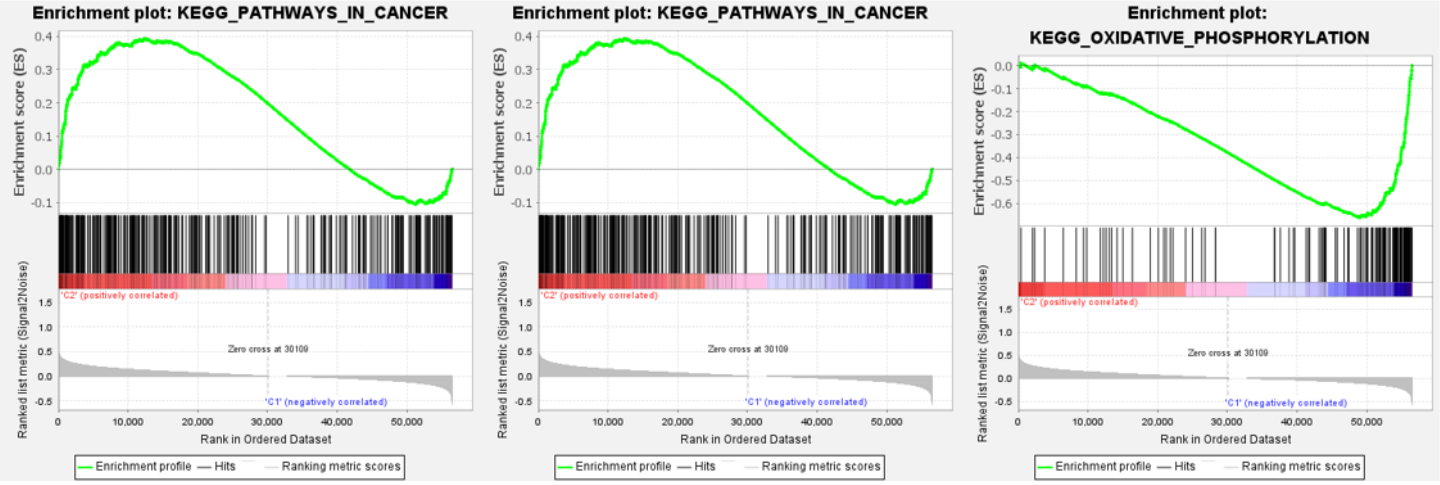

Figure 6

Results of CESC gene set enrichment analysis (GSEA).

Figure 7

Development of a Prognostic Signature. (A, B) Least absolute shrinkage and selection operator (LASSO) regression was performed, calculating the minimum criteria. (C, D) ROC (receiver operating characteristic) curves were used to evaluate the prediction efficiency of the prognostic signature. (E, F) The Kaplan–Meier survival analysis for train and test groups.

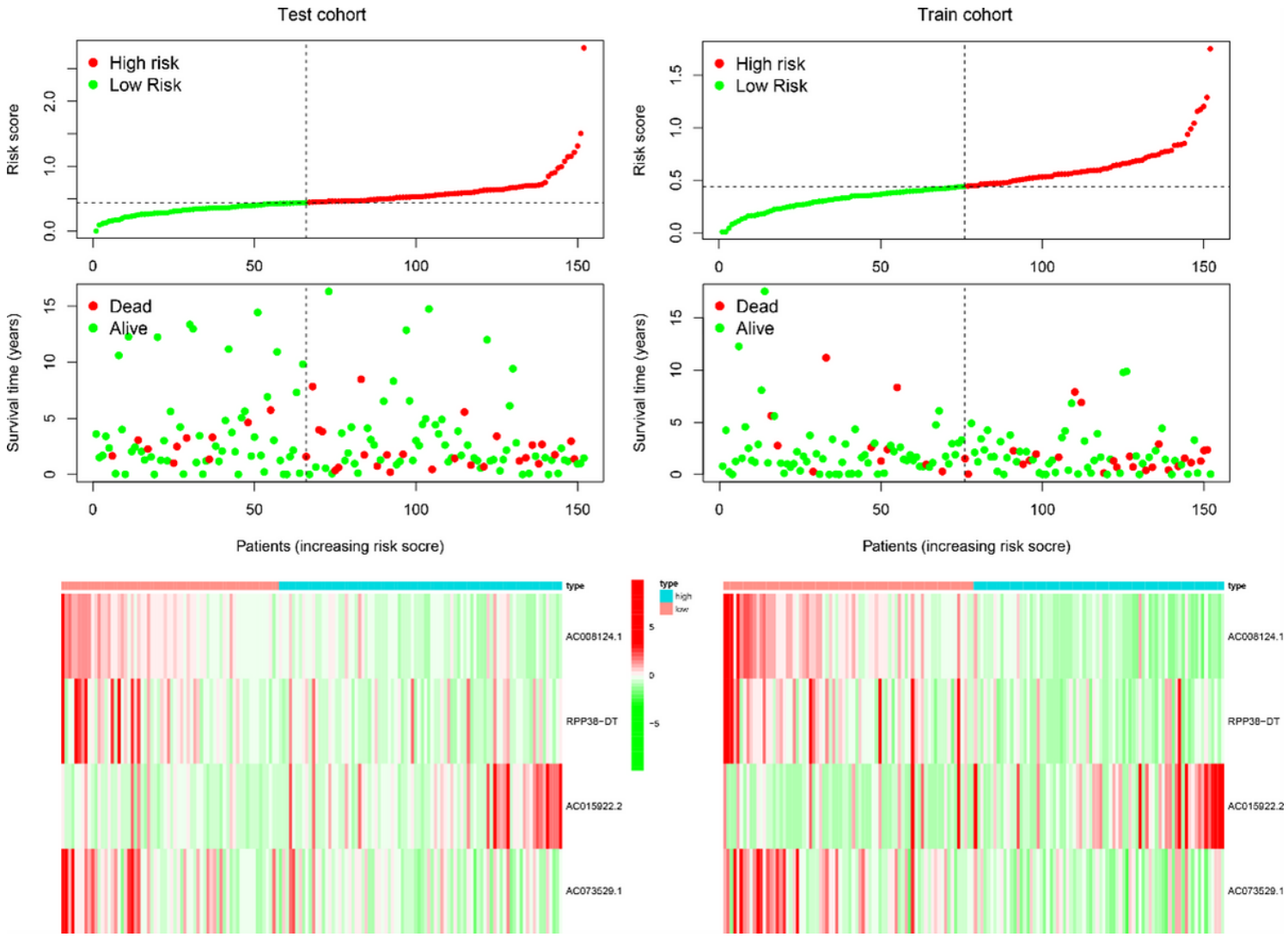

Figure 8

Distributions of risk scores (Red means high score risk, green means high score risk), survival status (Red means dead patients, green means alive patients) and risk heatmap (Red represents high expression, green represents low expression) of CESC patients based on the m6A-related lncRNA prognostic signature.

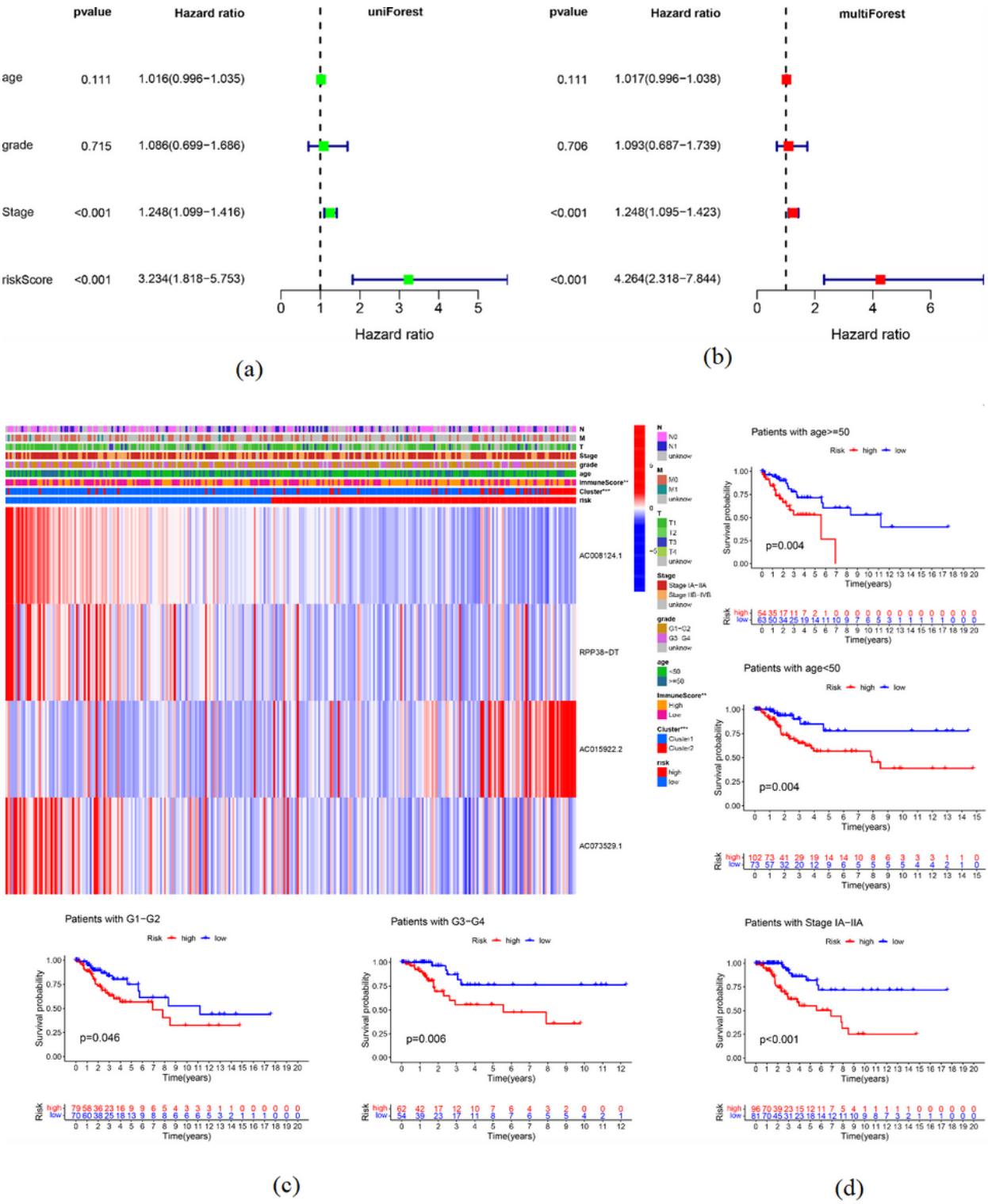

Figure 9

m6A risk scores as independent prognostic indicators. (A)Univariate Cox analysis of the clinicopathological features and risk score. (B)Multivariate Cox analysis identified the independent prognostic predictors. (C)The clinicopathological differences between the high- and low-risk groups. (D) Kaplan-Meier survival analysis of different clinical characteristics (patients age >=50/<50, patients with G1-2/3-4, patients with stage IA-IIA) in high-risk/low-risk groups.

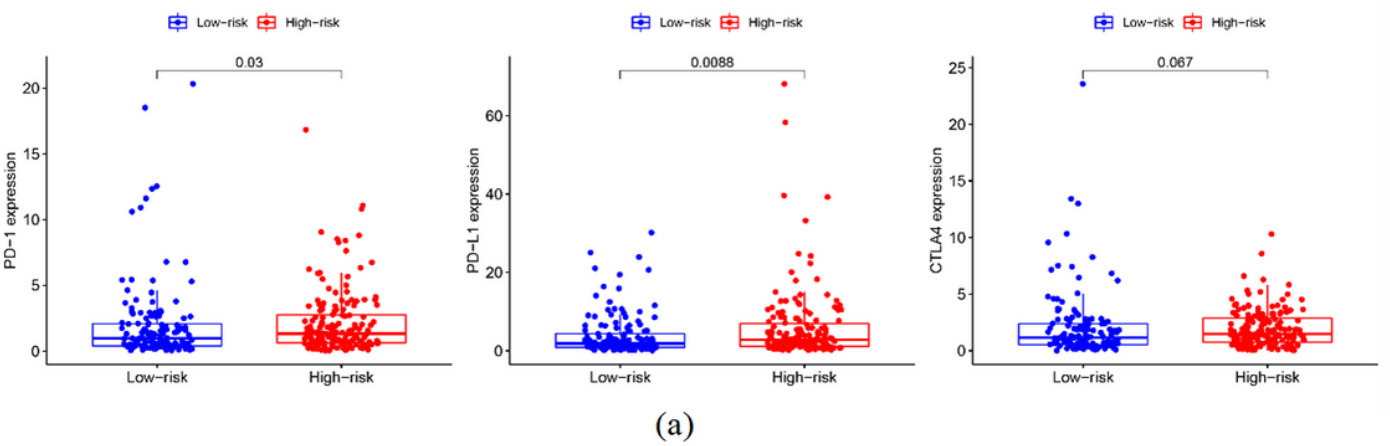

(a)

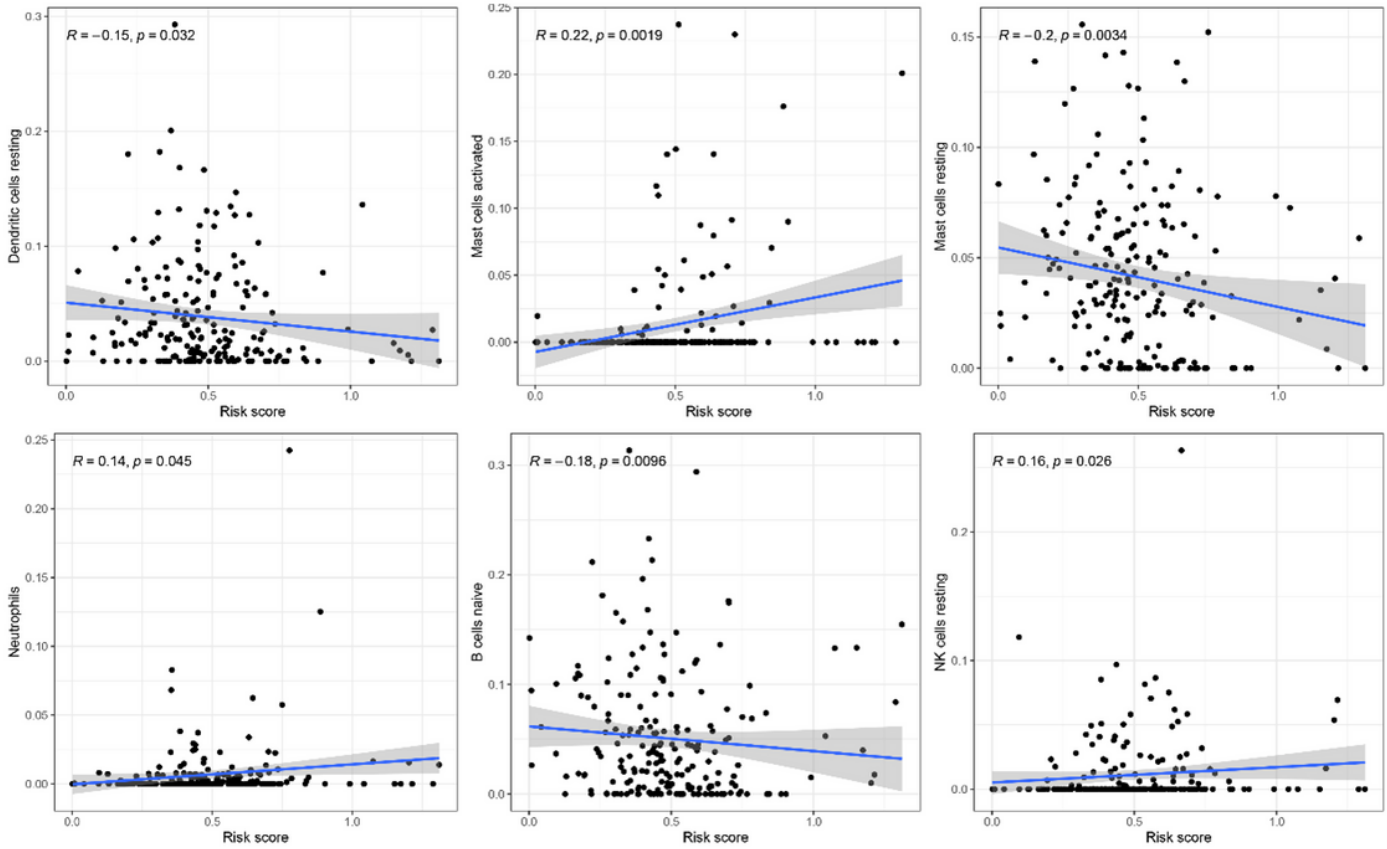

(b)

Figure 10

(A)m6A-related lncRNA modification on immune responses in CESC patients. (B)m6A-related immune cells in the tumor microenvironment in CESC patients.

Supplementary Files

This is a list of supplementary files associated with this preprint. Click to download.

- Additionalfile1.pdf
- Additionalfile2.xlsx